
Article:
Lu, X. orcid.org/0000-0001-6114-1964, Lian, G.J., Parker, J. orcid.org/0009-0009-4312-1949 et al. (4 more authors) (2024) Effect of carbon blacks on electrical conduction and conductive binder domain of next-generation lithium-ion batteries. Journal of Power Sources, 592. 233916. ISSN 0378-7753

https://doi.org/10.1016/j.jpowsour.2023.233916

Journal of Power Sources 592 (2024) 233916

Contents lists available at ScienceDirect

Journal of Power Sources

journal homepage: www.elsevier.com/locate/jpowsour

Effect of carbon blacks on electrical conduction and conductive binder domain of next-generation lithium-ion batteries

Xuesong Lu [a,b], Guo J. Lian [a], James Parker [a], Ruihuan Ge [a,b], Milan K. Sadan [a,b], Rachel M. Smith [a,b], Denis Cumming [a,b,*]

[a] Department of Chemical and Biological Engineering, University of Sheffield, Mappin Street, Sheffield, S1 3JD, UK
[b] The Faraday Institution, Quad One, Harwell Campus, Didcot, OX11 0RA, UK

HIGHLIGHTS

- Ratio of disordered to ordered carbon highly influences the electronic conduction.
- BET surface area highly influences the pore structure and ionic conductivity.
- Recommended ratio of carbon is 0.93–0.95 indicated by I_D/I_G of Raman spectroscopy.
- Recommended BET surface area is 130–200 m^2/g.

ARTICLE INFO

Keywords:
Lithium-ion electrode
Carbon black
Conductive binder domain
Rate capability

ABSTRACT

High energy and power density are key requirements for next-generation lithium-ion batteries. One way to improve the former is to reduce the binder and conductive additive content. Carbon black is an important additive that facilitates electronic conduction in lithium-ion batteries and affects the conductive binder domain although it only occupies 5–8% of the electrode mass. However, the function of the structure of carbon black on short- and long-range electronic contacts and pores in the electrode is still not clear and has not been systematically researched in detail. In this work, five carbon blacks with different BET surface areas, oil absorption numbers and ordered graphitic carbon content were investigated. It was found that the ratio of disordered amorphous carbon to ordered graphitic carbon in carbon blacks strongly influences the short- and long-range electrical conduction, and the BET surface area highly affects the pore structure and ionic conductivity in the electrode. Its optimum ratio, indicated by the Raman density I_D/I_G, is 0.93–0.95. The recommended BET surface area was 130–200 m^2/g for this experimental range. The results of this study can provide guidance for the screening of carbon blacks in the lithium-ion battery industry.

1. Introduction

Next-generation lithium-ion batteries (LIB) with high energy density (>350 kW/kg) and low cost (<£60/kW) are promising for the future development of electrical vehicles (EV) and energy storage devices. Lithium nickel manganese cobalt oxide, $LiNi_xMn_yCo_zO_2$ (NMC_{xyz}) is a pristine layered active material that can be utilised for next-generation LIBs. NMC has a high theoretical capacity (270 mAh/g for NMC622) [1] and the typical synthesis route produces spherical secondary particles of about 10 μm. To increase the energy density, there are ongoing efforts to minimise the content of inactive binder and carbon black. NMC has intermediary electrical conductivity compared to the electronically insulating active material LFP ($LiFePO_4$) and the highly electrically conductive active material LCO ($LiCoO_2$) [2]. For NMC, the electrical conductivity is state of charge (SOC) dependent and has an exponential decrease at higher Li contents (2–3 to 10^{-3} S/m) [3]. In LIBs, the conductive binder domain (CBD), consisting of conductive additives and polymer binder, is one of the important aspects that facilitates electron transfer and ion diffusion in electrodes. The CBD construction should be compatible with the features of next-generation LIBs with NMC as active material, which possesses larger particle size, intermediary particle conductivity, and a smaller quantity of conductive additive and binder

* Corresponding author. Department of Chemical and Biological Engineering, University of Sheffield, Mappin Street, Sheffield, S1 3JD, UK.
E-mail address: d.cumming@sheffield.ac.uk (D. Cumming).

https://doi.org/10.1016/j.jpowsour.2023.233916
Received 13 October 2023; Received in revised form 21 November 2023; Accepted 30 November 2023
Available online 12 December 2023

required (<4–6 mass%). CBD is an auxiliary structure for LIBs, but it plays a crucial role in dictating battery performance as it controls the electron and Li-ion transfer over the porous electrode. Conventionally, carbon black is favourable as a conductive additive because it is cheap and compatible with the generally used binder, PVDF (polyvinylidene fluoride) and solvent, NMP (N-methyl-2-pyrrolidone). Although some researchers have used carbon nanotubes (CNT) and graphene as conductive additives [4,5], their price is 10–100 times higher than that of carbon black [6]. Therefore, carbon black remains the best choice for the high-volume LIB manufacturing industry. Long et al. [7] published a detailed review of carbon blacks and other carbon materials. However, there are considerable types of carbon black powders so the challenge lies in the selection of the appropriate and optimum carbon black for NMC systems. To date, no detailed research or guidance has been published in the research field, so a specific standard is not available to be relied on when selecting the optimum carbon black. As such, this research aims to investigate the effect of carbon black types on short- and long-range electrical conduction and provide guidance for the carbon black and LIB manufacturing industries.

Carbon black typically exists as aggregates with a particle size of approximately 500 nm, consisting of primary spheroidal nanoparticles with a particle size of 30–50 nm [8]. For commercial carbon blacks, there are two important parameters to describe their characteristics: oil absorption number and BET surface area [9]. The oil absorption number is related to the void structure of carbon black. The void structure is created by the aggregation of primary nanoparticles with secondary particles, which causes the oil to be absorbed into these void spaces and effectively measures the structure of carbon black. The BET surface area is related to the primary particle size and a high surface area corresponds to a smaller primary particle size. The carbon black structure is an amorphous core surrounded by a shell of stacked graphene-like domains [10]. Thus, it can be seen that the ratio of disordered amorphous carbon to ordered graphitic carbon, oil absorption number and BET surface area are the key factors for characterising carbon black.

Raman spectroscopy is an effective tool to characterise carbon materials. The properties of carbon materials depend on the ratio of sp^2 (graphite-like, crystallite) to sp^3 (diamond-like, amorphous) bonds [11]. Generally, the Raman spectrum of carbon blacks shows two peaks: D band peak around 1350 cm^{-1} due to the breathing motion of sp^2 rings and G band peak around 1600 cm^{-1} due to the stretching of all pairs of sp^2 atoms in both rings and chains [12]. The intensity ratio of I_D/I_G is commonly used to evaluate the disorder of carbon networks and correlates linearly with the sp^2/sp^3 ratio [13]. Ferrari and Robertson [11,12] demonstrated that the variation of the intensity ratio of I_D/I_G can be divided into three stages: graphite to nanocrystallite graphite; nanocrystalline graphite to hydrogenated amorphous carbon; and hydrogenated amorphous carbon to tetrahedral amorphous carbon. Ostyn et al. [14] demonstrated that graphitization of carbon black causes the overall I_D/I_G to decrease, leading to a less asymmetric G band. On the other hand, when the graphitic carbon black becomes partly oxidized, I_D/I_G will increase. The ratios of I_D/I_G for graphite and graphene oxide are 0.04 and 0.86, respectively [15]. The ratio of I_D/I_G for common carbon blacks is in the range of 1.54–1.85 [16]. Shi et al. [17] produced a dual-confined SiO/carbon anode and found that the appropriate ratio of I_D/I_G for carbon is 1.05. This indicates that a lower intensity ratio of I_D/I_G represents a higher content of ordered graphitic carbon, and a higher intensity ratio of I_D/I_G represents a higher content of disordered carbon.

The purpose of carbon black addition into the LIB electrodes is to improve the electrical conductivity. The mechanism for increasing electron transport is percolation. When the concentration of carbon black in the insulation medium exceeds a critical value, the conductivity rises sharply [18]. The electrical conductivity above the percolation threshold can be described as

$$\sigma = \sigma_0 (V - V_c)^s \quad (1)$$

where σ is the conductivity of the mixture; σ_0 is the conductivity of the carbon black; V is the volume fraction of carbon black; V_c is the volume percolation concentration; s is a constant coefficient.

In the LIBs, there are two nested percolation systems: carbon black dispersed in polymer binder of PVDF and carbon black-PVDF composite dispersed among active material particles [19]. Generally, the carbon black and the binder constitute two CBD structures: a bridge structure that links two or more adjacent active material particles, and a film that covers the surface of the active material particles. Trembacki et al. [20] demonstrated that the bridge structure could improve electrode conductivity by 950%, which was much higher than that of the film structure. The structures constituted by carbon black and binder form the short- and long-range electronic contacts for electron transport.

On the other hand, the Li-ion transfer is also determined by the pore structure of CBD formed by carbon black. The formation of the CBD pore structure is strongly affected by the interaction between carbon black and the polymer. There are three polymer layers on the carbon black particles [21,22]: bounded polymer layer (about 5 nm thick), fixed or immobilized polymer layer (2–35 nm thick) and excessive or free polymer. It has been demonstrated that the colloidal forces between carbon black particles in the slurry dominate the rheological properties and subsequent electrical performance [6,23,24]. The total colloidal force is a function of the steric repulsion force from polymer coating, the van der Waals attraction force and the electrostatic double layer repulsion force due to the particle surface charge [7,25,26].

The surface distance between two carbon black particles, which is determined by the colloidal forces, is a function of the adsorbed polymer brush length. On the other hand, stretching of the polymer chain can form the voids. Through drying, the floc structures become CBD structures and may result in two types of pores: large pores derived from the gap of particles in the colloid and small pores from polymer chain stretching assisted by the carbon black particles [19]. The two nested pore systems greatly influence Li-ion diffusion in the CBD and thus affect the performance of LIBs. In summary, carbon black not only determines the conductivity of the electrodes but also controls the slurry rheological properties during electrode fabrication and colloid structure with the binder PVDF, which further affects the formation of CBD and ion transfer in LIBs. Three parameters of carbon blacks, including the ratio of disordered carbon to ordered graphitic carbon, which may be related to the electrode conductivity; oil absorption number, which may be connected to the polymer absorption in the void structure of secondary carbon black aggregates; and BET surface area which may be relevant to particle percolation, are the most important keys to LIBs.

Currently, there are some studies on the effect of carbon black on LIBs. Spahr et al. [27] studied carbon blacks C-NERGY™ Super C65 and C45, Super P® Li, Super S® and acetylene black with BET areas of 45–72 m^2/g for LIBs. Using a two-point electrical resistivity measurement, it was found that C45 dry mixed with $LiCoO_2$ powder had the lowest electrical volume resistivity and highest compressibility. The reason is that C45 has a lower degree of graphitization and a higher concentration of oxide groups. Although the findings recommend carbon black C45 for LIB applications, carbon black C65 as conductive additive is still widely used with no clear justification given [28–31]. Qi et al. [9] investigated the influence of the surface area of conductive carbon additives on the performance of $LiFePO_4$ LIBs. Five carbon blacks with the BET surface areas of 53–580 m^2/g were selected and investigated. It was found that the LIB performance, such as electrical conductivity and discharge capacity, was greatly influenced by the surface area, particle size and morphology of the carbon additives. The best rate performance was achieved with carbon black with a specific surface area of 180 m^2/g. To the best of our knowledge, only this publication provides a parameter for suggesting the use of carbon black. Marinho et al. [32] compared the electrical conductivities of graphene, multi-wall carbon nanotube, carbon black and graphite powders in a load cell and found that the conductivities at high pressure (5 MPa) for the

graphene, nanotube and carbon black were given as lower values (~10^2 S/m) but the conductivity of graphite can reach ~10^3 S/m. Kwon [33] used ball mixing of $LiCoO_2$ with platelet-shaped graphite (SFG), spherical graphite (SLC), carbon black Ketjenblack 600 and C-NERGY™ Super C65 to investigate the effect of carbon black morphology on LIBs. They found that platelet-shaped graphite SFG provided well-defined redox peaks with narrow anodic and cathodic peaks but spherical graphite SLC and carbon black Ketjenbalck 600 with high surface area provided broad redox peaks and a larger potential difference between the anodic and cathodic peaks, which means a higher reactivity of the electrode. Cho et al. [34] compared carbon black Super® P with vapor-grown carbon fibres (VGCFs) as conductive additives for LIBs. Hwang et al. [35] used functionalized rGo (reduce graphene oxide) and carbon nanotubes coating on $LiNi_{0.8}Co_{0.1}Mn_{0.1}O_2$ as the cathode. Chen et al. [4] adopted carbon black Super® P, carbon black 350G, carbon nanotube and graphene as the conductive additives for $LiNi_{0.5}Co_{0.2}Mn_{0.3}O_2$. Liu et al. [36] constructed hierarchical carbon nanotube/carbon black scaffolds as the short- and long-range electron pathway for LIBs. Gong et al. [37] reviewed one-dimensional carbon such as carbon nanotubes and carbon fibres, two-dimensional carbon such as graphene, graphene oxide and reduced graphene oxide, and three-dimensional carbon such as carbon nanotube array and graphene skeleton modified $LiFePO_4$ as the cathode for high power LIBs. Wang et al. [38] built a hybrid super-aligned carbon nanotube/carbon black conductive network for LIBs. All the literature mentioned above exclusively studied the influence of different carbon materials on battery performance but did not propose the mechanism of the action of these materials in detail. It can be seen that although the publications on carbon blacks for LIBs are abundant, the systematic study on the structure and surface of carbon black influencing the performance of LIBs has rarely been reported. As a result, there is no indication of what carbon black parameters would be suitable for LIBs applications.

The purpose of this work is to systematically study the influence of carbon black properties on the structure of CBD and the electron and ion transfer, so as to propose optimised carbon black parameters and provide a basis for the selection of carbon black for LIBs. This contribution aims to summarise and propose the mechanism of how different parameters of carbon black regulate CBD structure and the performance of LIBs. In this study, we chose five commercial carbon black powders with different oil absorption numbers and BET surface areas to investigate how they affect the performance of next-generation LIBs based on the active material $LiNi_{0.6}$ $Mn_{0.2}Co_{0.2}O_2$ (NMC622). NMC622 was selected as a standard model of active material in the "Nextrode" project due to its excellent performance, high capacity and energy density, relatively low cost, good stability, and safety.

2. Experimental materials and methods

See the supplementary information.

3. Results and discussions

3.1. Characterisation of different carbon black particles for electrode conduction

First, the carbon blacks were characterised by TEM and Raman spectroscopy to evaluate their morphology and ratio of disordered carbon to ordered graphitic carbon. Fig. 1(a–e) shows TEM images of different carbon blacks. The particle size was determined from TEM images by randomly selecting 10 particles and averaging. The average primary particle sizes are 50, 32, 25, 20 and 10 nm for carbon blacks C45, C65, LHP, L200 and L300, respectively, corresponding to the increase of the BET surface area as shown in Table S1. It can also clearly be seen that the disordered carbon is located in the core and the ordered graphitic carbon is located in the outer shell as shown in Fig. 1(f) with carbon black L300. The ratio of disordered carbon and ordered graphitic carbon for the different carbon blacks is shown in Fig. 2.

The Raman spectrum of different carbon blacks is shown in Fig. 2(a)

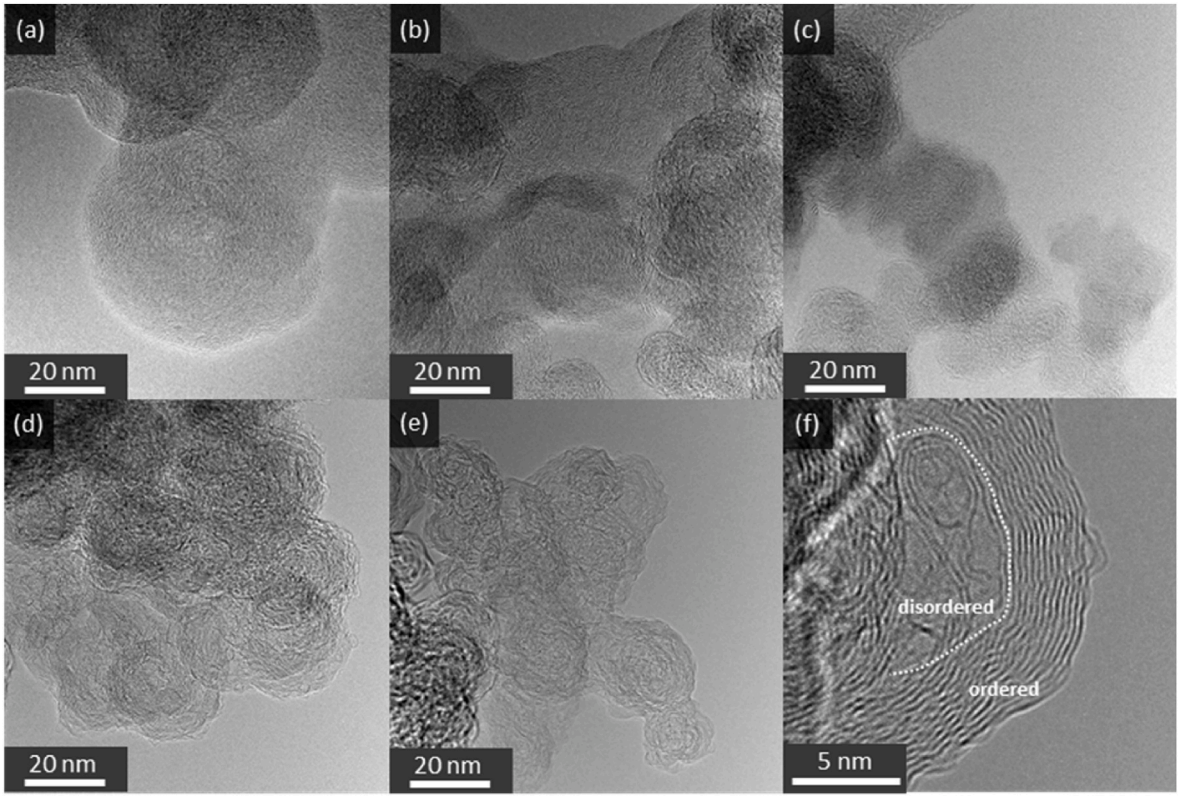

Fig. 1. TEM images of different carbon blacks (a) C45; (b) C65; (c) LHP; (d) L200; (e) L300; (f) L300 with an ordered shell and a disordered core.

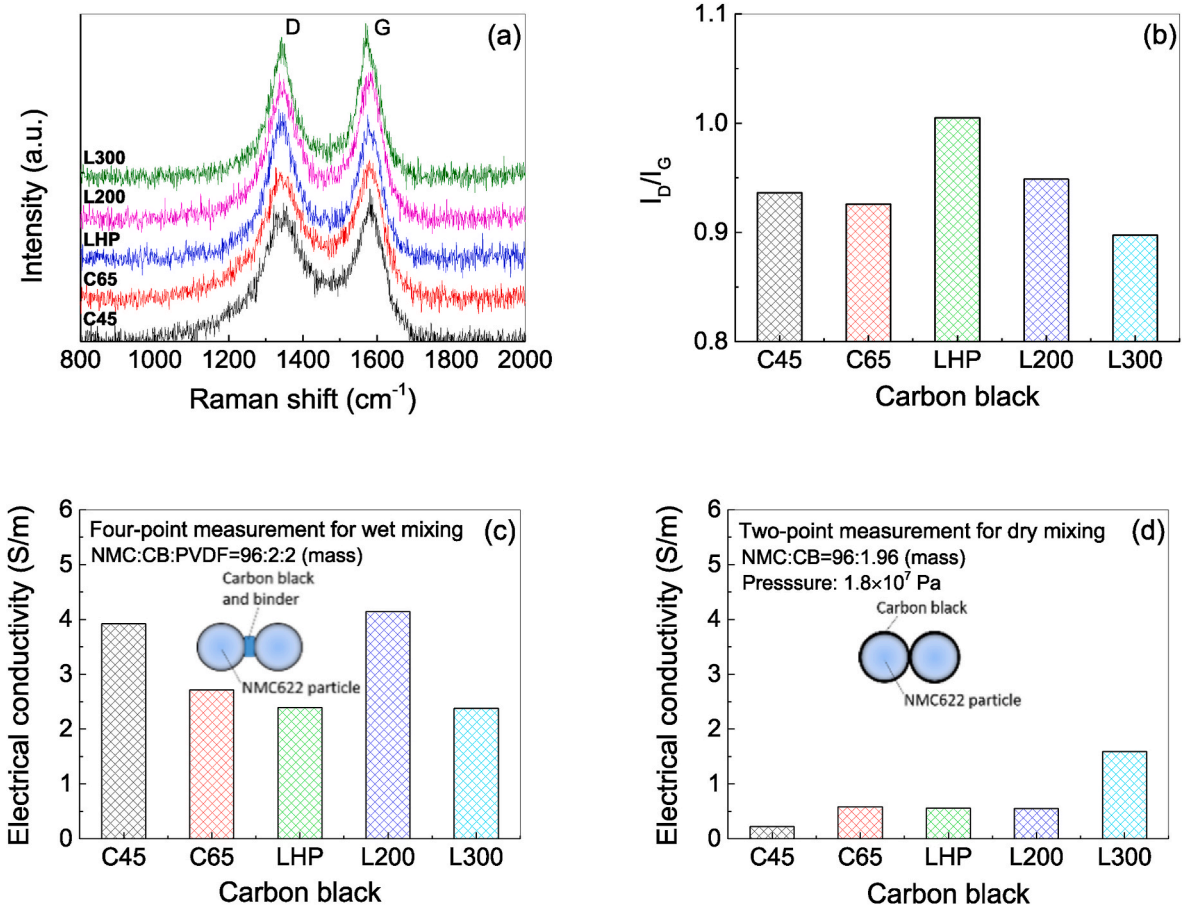

Fig. 2. Raman spectroscopy of carbon black powders and electrical conductivity (a) Raman spectrum; (b) intensity ratio of I_D/I_G; (c) electrical conductivity of thin film measured by the four-point method (thin film prepared by wet slurry mixing and casting on a PET film); (d) electrical conductivity of packed powder measured by the two-point method (NMC particles coated by carbon blacks under dry mixing mechanofusion).

where the distinct *D* and *G* band peaks for all carbon blacks are visible. The intensity ratio I_D/I_G is shown in Fig. 2(b) and carbon black LHP has the highest I_D/I_G of more than 1.0, indicating the highest fraction of disordered carbon among all carbon blacks studied. L300 has the lowest I_D/I_G, indicating that it has the highest fraction of ordered graphitic carbon. Among the carbon blacks with I_D/I_G less than 1.0, C45 and L200 have a relatively high intensity ratio of I_D/I_G, suggesting that these two carbon blacks have a relatively high fraction of disordered carbon. Pantea et al. [39] pointed out that the electrical conductivity of the carbon black increases with the graphitic character of the surface, but for low surface area conductive carbon blacks, the electrical conductivity correlates well with the surface chemistry. The fraction of ordered graphite carbon should be related to the conductivity of the electrode, e.g. the long-range and short-range electronic contact.

Entwistle et al. [40] defined long-range electronic contacts as the interconnected percolation network that spans between the active material particle in the 0.1–10 μm range and short-range electronic contacts are the nearest neighbour interactions between CBD and active material particle on the 1–100 nm length scale. The long-range electronic contact is formed by the wet mixing of PVDF, carbon black and active material particles in the solvent of NMP. The short-range electronic contact is formed by high-intensity dry mixing of active material particles with carbon black.

The electrical conductivity of the electrode in Fig. 2(c) was determined using the four-point method for thin films [41], corresponding to the long-range electronic contact established by wet mixing with active material particles linked by CBD for enhanced electron transfer. To rule out the effect of the current collector on the conduction of the film, the electrode was prepared by coating the slurry on a PET film without subsequent calendering. The equation for the electrical conductivity (σ) is:

$$\sigma = \frac{I}{ln(2)\Delta V t} \tag{2}$$

where I is the current between two outer probes; ΔV is the voltage between two inner probes; t is the thickness of the coated film.

The thickness of the coated films is 73, 65, 63, 54 and 65 μm for the electrode with carbon black C65, C45, LHP, L200 and L300, respectively with a porosity of approximately 0.5. The results show that the electrical conductivity increases from 2.4, 2.4, 2.7, 3.9 to 4.1 S/m corresponding to the electrodes prepared by carbon black from L300, LHP, C65, C45 to L200, respectively. Among the carbon blacks with I_D/I_G of less than 1, L300 has the most ordered graphitic carbon components, but the electrical conductivity of the electrode is the lowest. On the contrary, although C45 and L200 have more disordered carbon, the electrical conductivities of the electrodes are the highest. One possible reason is that the disordered carbon is compatible with PVDF and NMP, and conducive to the formation of an effective percolation system while the ordered graphite carbon is less compatible with PVDF and NMP. This phenomenon may be due to the dispersibility of carbon black in the slurry. Ali et al. [42] pointed out that high electrical conductivity of carbon black is known to be possessed only by the grades that have a high surface area, high structure, and lower proportion of polar groups, which consequently results in poor dispersibility. Therefore, there is a dilemma between high electrical conductivity and dispersibility.

The electrical conductivity of the carbon black-coated NMC622

particles in Fig. 2(d) was measured by the two-point method by compressing particles in a load cell [27]. This corresponds to short-range electronic contacts established by dry mixing of active material particles directly with carbon black for enhanced electron transfer. The equation for the electrical conductivity (σ) is

$$\sigma = \frac{I}{\Delta V}\frac{L}{A} \tag{3}$$

where L is the height of packed particles; A is the cross-sectional area of the press die.

The electrical conductivities for the packed powders are 0.22, 0.58, 0.56, 0.55 and 1.59 S/m for NMC622 particles dry coated with C45, C65, LHP, L200 and L300, respectively. The measured short-range contact conductivities in Fig. 2(d) are much lower than the long-range contact conductivities in Fig. 2(c). This may demonstrate that the long-range electronic contact is more important than the short-range contact. The NMC622 particles coated with carbon black L300 have the highest conductivity which is likely due to the highest ordered graphite fraction in carbon black L300. Similarly, the NMC622 particles coated by C45 and L200 gave a relatively low conductivity due to the low content of ordered graphitic carbon. This indicates that the carbon black with more ordered graphitic carbon facilitates the establishment of short-range electronic contact by dry mixing.

The oil absorption number of carbon black increases from L300, L200, LHP, C65 to C45 while the BET surface area of carbon black increases from C45, C65, LHP, L200 to L300 but the trend of the electrical conductivity for the electrodes with different carbon blacks is distinctly different from the trend of oil absorption number and BET surface area of carbon blacks. It shows that the electrical conductivity of the electrode is not strongly correlated with the oil absorption number and BET surface area of carbon blacks, but is closely related to the ordered graphitic carbon in carbon black.

From the above experimental results, it can be concluded that the electrical conductivity of long-range or short-range electronic contact has a direct correlation with the ratio of disordered carbon to ordered graphitic carbon in carbon blacks.

3.2. Characterisation of slurries with different carbon blacks

This section studies the rheological properties of the slurries with different carbon blacks. There are two main purposes: one is to study the effect of carbon black oil absorption number on the binder PVDF, which represents the function of particle aggregate void structure on the absorption of PVDF into the carbon black; the other is to study the interaction between disordered carbon and PVDF.

The rheological properties of slurries with different carbon blacks are shown in Fig. 3(a) and (b). Fig. 3(a) displays that under a low shear rate, the slurries with carbon black C45 and L200 have a relatively low viscosity, e.g. at a shear rate of 1 s^{-1}, the viscosity is 0.78 and 0.89 Pa·s respectively for slurries with C45 and L200. The viscosities for the slurries with C65, LHP and L300 are relatively higher, e.g. at a shear rate of 1 s^{-1}, the viscosity is 10.36, 8.50 and 4.62 Pa·s for slurries with C65, LHP and L300, respectively. Fig. 3(b) indicates that the storage moduli for the slurries with C45 and L200 are relatively low, and with increasing shear strain in the range of 0.1 and 20%, the storage modulus is nearly constant around 0.15 and 1.02 Pa. The slurry with C65 has a relatively high storage modulus of around 3 Pa even at low shear strain, but with increasing shear strain, the storage modulus slightly increases. The curves of storage modulus vs. shear strain for the slurries with LHP and L300 retain the same trend and with increasing shear strain, the storage modulus increases greatly from about 1 Pa to 6 Pa. It is worth

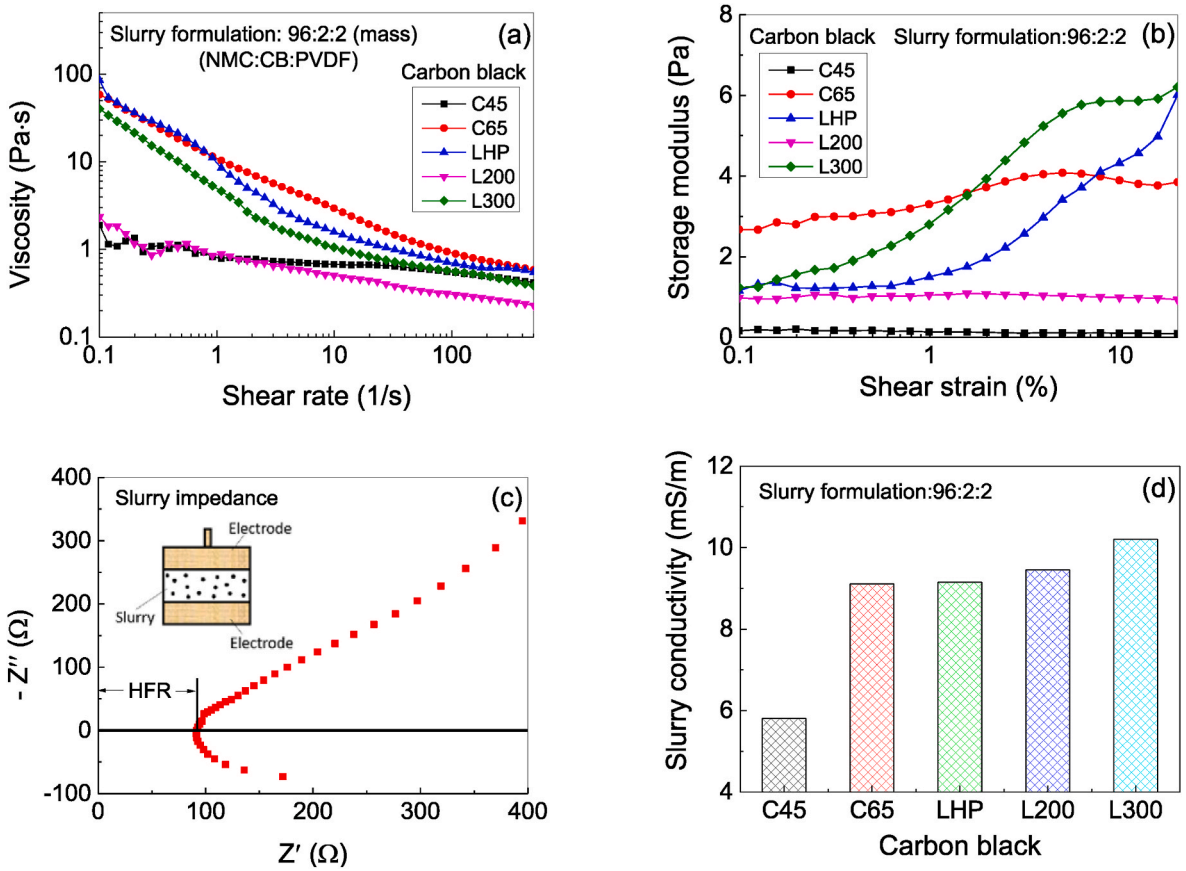

Fig. 3. Slurry rheological properties and conductivities with different carbon blacks (a) viscosity; (b) storage modulus; (c) impedance of slurries; (d) conductivity of slurries.

highlighting that carbon black L300 with more ordered graphitic carbon content induces higher viscosity and a stronger storage modulus. It has also been shown in other literature that ordered graphitic carbon has a stronger effect on polymers [43]. It is well known that in a slurry, a small amount of ordered graphitic carbon achieves a higher viscosity and storage modulus than other solid particles [44,45].

From the current results, there is no strong favourable rule between the rheological properties and the oil absorption number of carbon blacks. It indicates that the rheology of the slurry has little connection with the oil absorption number of carbon blacks. However, the viscosity of the slurry has a strong relationship with the ratio of disordered carbon to ordered graphitic carbon in carbon blacks. For carbon blacks with I_D/I_G less than 1, carbon blacks with more disordered carbon, e.g. carbon black C45 and L200, obtained low viscosity and storage modulus. Carbon black with more ordered graphitic carbon, e.g. carbon black L300, achieved high viscosity and storage modulus. Careful analysis reveals that the change in viscosity for different slurries is intrinsically linked to the electrical conductivity of the electrode measured by the four-point method. Lower slurry viscosity correlates to higher electrical conductivity whereas higher slurry viscosity correlates to lower electrical conductivity. The rheological results discussed are linked to the results of conductivity in Section 3.1 where the rheological properties of slurries are strongly linked to the ratio of disordered carbon to ordered graphitic carbon in carbon blacks.

Electrochemical impedance spectroscopy (EIS) is often used to characterise solid electrodes in the context of a cell. However, it is useful to characterise the conductivity of LIB electrode slurry to observe the evolution of electrical conductivity from liquid slurry to solid electrode [46]. The slurry resistance (R_{HF}) is evaluated from the real component of impedance that intersects with zero imaginary in high frequencies (HFR) [47,48]. The typical measured impedance of an electrode slurry is shown in Fig. 3(c) and the equation is shown in the following.

$$\kappa_s = \frac{1}{R_{HF}} \frac{L}{A} \tag{4}$$

where L is the thickness of the slurry in the sample holder; A is the area of the measurement electrode.

The results of slurry conductivity are shown in Fig. 3(d). The conductivities of slurries estimated according to Equation (4) are 5.81, 9.11, 9.15, 9.46 and 10.21 mS/m for carbon blacks C45, C65, LHP, L200 and L300, respectively. It was found that the slurry conductivity increases with decreasing carbon black particle size. This shows that smaller carbon black particles are beneficial to the conductivity of the slurry. Liang and Yang [49] found that a larger surface area and smaller particle size are favourable for the conductivity of the composite filled with carbon blacks. Jing et al. [50] explained the effect of particle size on electrical conducting percolation in composites. The smaller particle size results in an increase in particle number per volume [51]. The inter-particle distance decreases proportionally with decreasing particle diameter. When the inter-particle distance is shorter than the gap width that quantum tunnelling effect permits, the percolation phenomena will occur.

Hence, the rheological properties of the slurry are strongly related to the ratio of disordered carbon to ordered graphitic carbon, and the slurry conductivity is strongly influenced by the particle size of carbon blacks. According to this theory, carbon black L300 has the smallest particle size and the largest specific surface area among these carbon blacks and should possess high electrical conductivity, but the measured electrical conductivity is lower. The possible reason is related to the secondary agglomeration or the generated defective bridge structure during the drying process after coating. The bridge is formed by surface tension to the contact point or capillary tube of active material particles and the contact angle of the slurry on the surface of active material particles.

3.3. SEM characterisation of the electrodes with different carbon blacks for CBD structures

It is universally agreed that the conductive binder domain (CBD) is a critical aspect of LIB cathodes because it significantly influences electron transfer and ion diffusion. The formation of CBD structures is strongly related to the slurry colloid and drying process. Different carbon black particles form different colloid structures in the slurries due to interaction forces among carbon black surface functional groups, binder PVDF and solvent NMP, which affect the quantity of polymer absorbed by carbon black particles and the polymer brush length on the particle surface. The drying process causes PVDF and carbon black to migrate to the capillary pores formed by the accumulation of NMC622 particles and subsequently move to the surface of the electrode with solvent evaporation.

Fig. 4(a), (c), (e), (g) and (i) shows the SEM images of the different carbon black CBD structures from top view. These CBD structures resemble a “fluffy, sponge-like” structure. This morphology is related to the chain extension of the polymer in the solvent under the action of carbon black. The “fluffy, sponge-like” appearance may be caused by the vapor-induced phase separation [52,53]. From these figures, it is apparent that the effect of different carbon blacks on PVDF is different because the size of the voids of the formed “fluffy, sponge-like” structure is different. The void in the CBD structure formed by carbon black C45 is the largest, followed by carbon black C65, L200, L300, and finally LHP. The CBD formed by carbon black LHP is the most compact while the CBD formed by carbon black C45 is the loosest. The bridge structures appear near the packed particle contact points. The dense CBD formed by carbon black LHP and PVDF results in a small bridge structure. The loose CBD structures formed by carbon black C45 and PVDF resulted in a bridge structure that represents carbon “sponge” filled in the spaces between the NMC622 particles. Spahr et al. [27] reported that there is a higher concentration of oxygenated hydrocarbon and carboxylic acid functional groups in the carbon black C45. These functional groups of the carbon black cooperate with the functional groups of the polymer to influence the stretching of the polymer chain through solvent evaporation, resulting in a longer brush length, so the carbon sponge forms a loose structure for carbon black C45. Only the carbon blacks of C65, L200 and L300 and polymer PVDF obtain stable bridge structures over the gap between NMC622 particles.

The SEM images in Fig. 4(b), (d), (f), (h) and (j) show the distribution of NMC622 particles from cross-sectional view. The specimens were filled with Epofix resin for microtome surface grinding. From the cross-section of the electrodes, there are no significant differences in the arrangement of NMC622 particles between different electrodes. This shows that carbon black has little effect on the distribution of NMC622 particles in the electrode. The main reason may be that the diameter of NMC622 particles (around 10 μm) is much larger than the diameter of carbon black (around 5–30 nm) so NMC622 particles dominate the accumulation and arrangement of particles during the drying process.

As the electrode film was filled with the Epofix resin for microtome grinding, the true CBD distribution could not be directly distinguished from the SEM images of the electrode cross-section. However, since PVDF contains fluorine, EDS fluorine mapping can express the distribution of CBD, including carbon black, by fluorine distribution along the electrode cross-section. Fig. 4(k) and (l) show the fluorine mapping images of electrodes with carbon black L200 and LHP, respectively. It can be seen from these two images that CBDs are mainly concentrated in the pores smaller than 2 μm and rarely appear in the pores larger than 2 μm. This might be attributed to the result of the binder migrating into these small pores driven by the capillary force during the drying process.

3.4. MIP pore characterisation of electrodes with different carbon black for Li-ion transfer

The ionic conductivity is determined by the electrode pore condi-

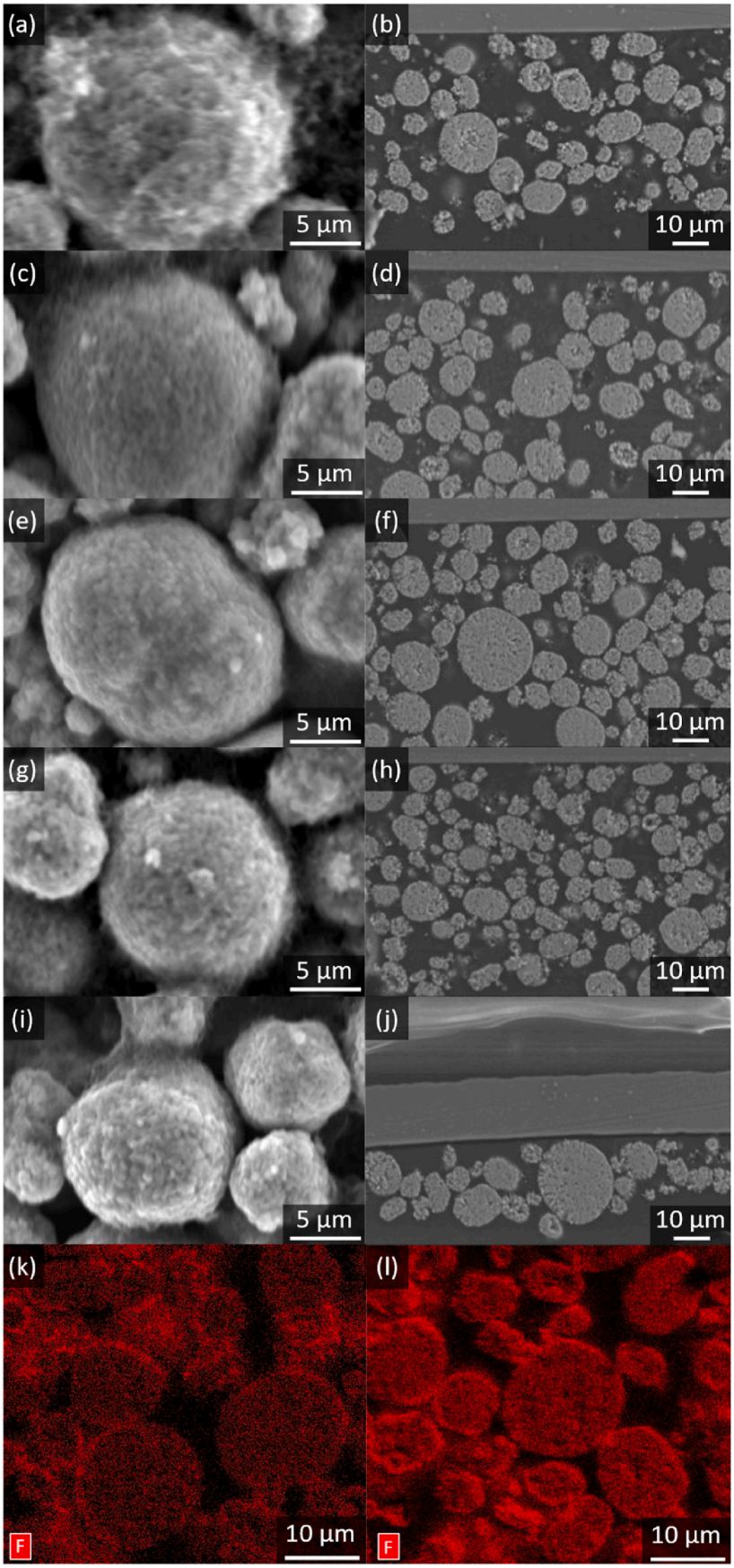

Fig. 4. SEM images (top view, magnification: 5000 and cross-section, magnification: 1200) and EDS fluorine mapping of electrodes prepared from different carbon blacks (NMC622:CB:PVDF) (a)(b) C45; (c)(d) C65; (e)(f) LHP; (g)(h) L200; (i)(j) L300; EDS mapping (k) L200; (l) LHP.

tions. The relationship between ionic conductivity and pores in the electrodes is shown in the following equation.

$$\kappa = \kappa_0 \left(\frac{\varepsilon}{\tau}\right)^b \quad (5)$$

where κ is the ionic conductivity; κ_0 is the free constant ionic conductivity; b is a constant coefficient; ε is the porosity; τ is the tortuosity of the electrode.

The pore distributions of uncalendered and calendered electrodes with different carbon blacks are shown in Fig. 5. Fig. 5(a) indicates that there are two types of pores: large pores in the electrodes (around 3 μm) and small pores in the CBD (around 100 nm) which is in agreement with literature [54–56]. There is such a trend for the electrodes with different carbon blacks. With the reduction of particle size or the increase of BET area for different carbon blacks, the pore size of the small pores in the CBD becomes smaller and the pore size of the large pores in the electrodes becomes larger. For example, the pore sizes of small pores for electrodes (peak of the pore size distribution below 0.5 μm) with C45 and L300 are 500 and 68 nm, respectively; the pore sizes of large pores for electrodes with C45 and L300 are 2.5 and 3.2 μm, respectively. However, there is an outlier which is the electrode with carbon black L200. Although the particle diameter of the carbon black L200 is smaller than that of LHP, the pore sizes of large and small pores for the electrode with L200 are between that of the electrode with C65 and LHP. One possible reason is that the dispersion of carbon black L200 in the PVDF and NMP is not satisfied. Through calendering, the pore size distribution shifted to a smaller size as shown in Fig. 5(b). This shows that calendering mainly reduces the proportion of large pores in the electrode and

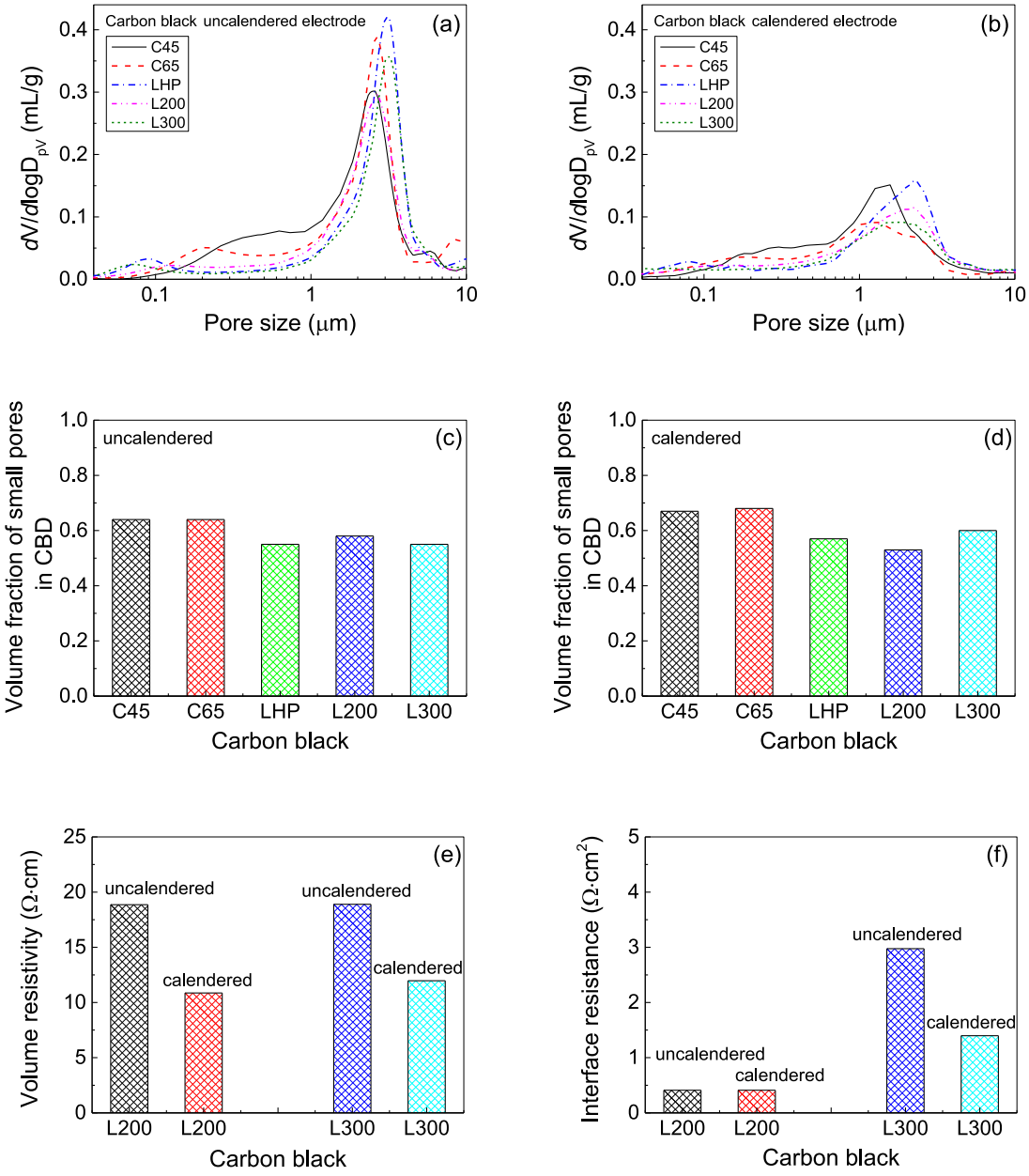

Fig. 5. Pore size distributions of electrodes, volume fraction of small pores in CBD with different carbon blacks and comparison of volume resistivity and interface resistance (a)(c) uncalendared pore distribution; (b)(d) calendered pore distribution; (e) Comparison of volume resistivity between calendered and uncalendared electrode; (f) comparison of interface resistance between calendered and uncalendered electrode.

shifts the pore size distribution to the left with a smaller size.

By defining small pores as pores with a size less than 0.5 μm, the volume fractions of small pores in CBD with different carbon blacks before and after calendering are shown in Fig. 5(c) and (d). Before calendering, the volume fractions of small pores in CBD with carbon black C45 and C65 are slightly higher than those with LHP, L200 and L300. All the volume fractions of small pores in CBD are around 0.60 before calendering as shown in Fig. 5(c). After calendering, the volume fraction of small pores in CBD slightly increases by 0.02–0.04 as shown in Fig. 5(d). This is because the pore size distribution was shifted to a smaller size by calendering. However, it was further demonstrated that calendering affected small pores in the CBD very slightly and mainly reduced the volume of large pores.

In this work, the volume resistivity and interface resistance were measured by the Hioki RM2610 electrode resistance measurement system. Through these measurements, it was demonstrated that calendering could decrease the volume resistivity and interface resistance. The volume resistivity of the electrode with L200 before and after calendering is 18.86 Ω cm and 10.86 Ω cm, respectively. The interface resistance of the electrode with L300 before and after calendering is 2.98 Ω cm^2 and 1.40 Ω cm^2 respectively as shown in Fig. 5(e) and (f). The interface resistance for the electrode with carbon black L200 decreases very slightly after calendering. The reason might be that, although the contact area could be increased through the binder network compression, sometimes the displacement of active material particles caused by less mechanical strength can lead to contact loss between the current collector and electrode film [57]. For the electrode with L200, the factors for increasing and decreasing interface resistance are compromised.

Calendering reduces the porosity of the electrode, which is unfavourable for ion diffusion. However, calendering increases the surface area per unit volume, which is beneficial to the electrochemical reaction processing on the surface of active material particles [58]. It can be seen from Fig. 5(e) and (f) that calendering also reduces the volume resistivity and interface resistance of the electrodes. The effect of carbon black on the electrodes is mainly in the small pores of CBD. Different carbon black particle sizes lead to different pore sizes of CBD, which affect ion diffusion.

3.5. Impedance of the coin half cell

Electrochemical impedance spectroscopy (EIS) can be used to evaluate the electrolyte resistance and charge transfer resistance of a cell. The impedance curves of the coin half cells based on different carbon blacks are shown in Fig. 6(a) and the equivalent circuit is shown in Fig. 6 (b). The parameters of these coin half cells are listed in Table 1. Fig. 6(a) displays the electrodes with carbon black C65, L200 and L300 have small single semi-circles while the electrodes with C45 and LHP have relatively large single semi-circles. The equivalent circuit which was designed according to literature [59–61], consists of an inductor (L) which is related to the wiring and instrument, a resistor (R_s) standing for the resistance from electrolyte, a resistor (R_{ct}) for the charge transfer resistance at the interphase between electrode and electrolyte, a constant phase element (CPE_{dl}) for the double layer between electrode and electrolyte, and a constant phase element (CPE_{diff}) for the impedance of diffusion. The definition of the constant phase element is

$$Z_{CPE} = \frac{1}{CPE_T(j\omega)^{CPE_P}} \tag{6}$$

The charge transfer resistance decreases from 100.10, 90.00, 64.23,

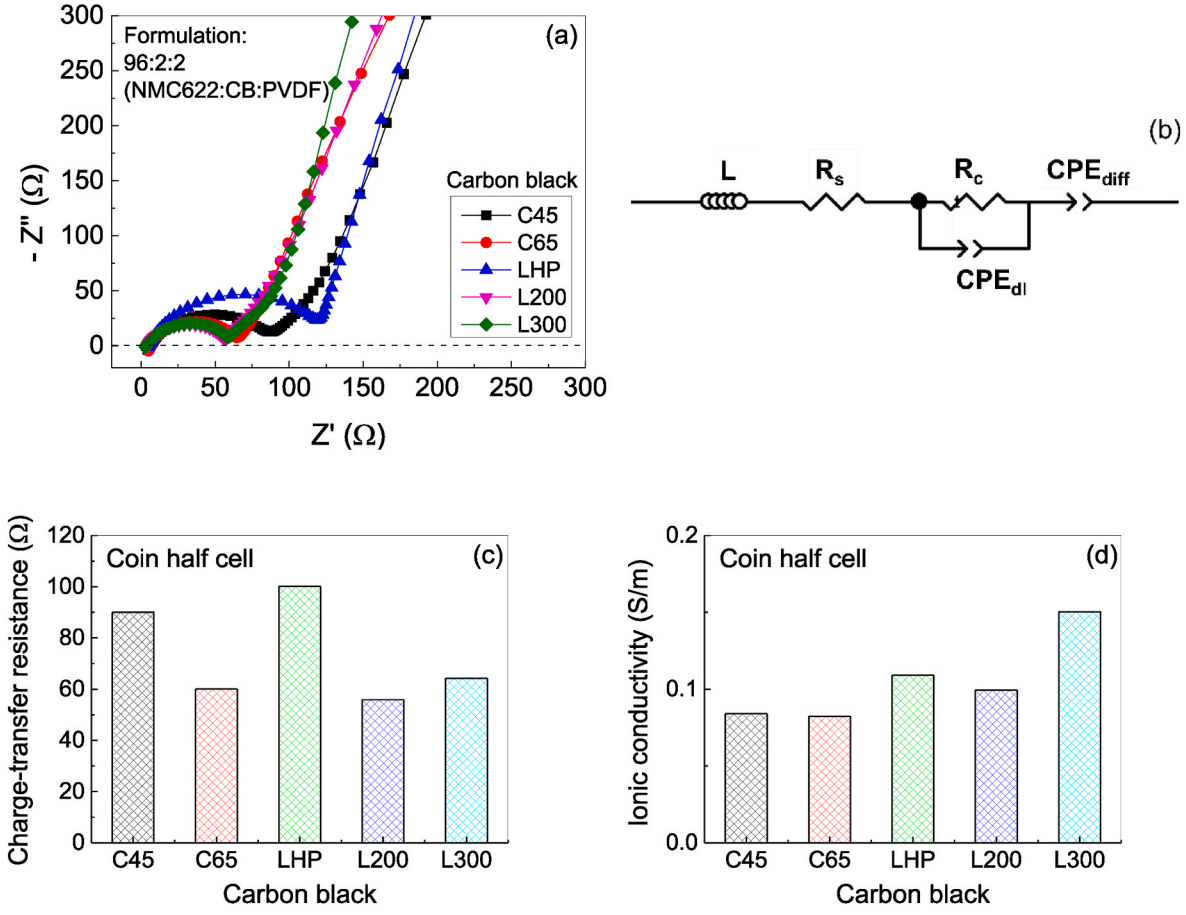

Fig. 6. Impedance of the electrodes based on different carbon blacks. (a) Impedance; (b) Equivalent circuit; (c) Charge transfer resistance; (d) Ionic conductivity.

Table 1
Electrode parameters of coin half-cell fabricated from different formulations.

Carbon black	Diameter (mm)	Thickness (mm)	Mass (mg)	Area mass (g/m^2)	Porosity before calend.	Porosity after calend.	Capacity (mAh/cm^2)	C-rate (mAh)
C45	14.8	0.098 (0.079)[a]	38.52	183	0.51	0.36	2.94	5.28
C65	14.8	0.112 (0.089)[a]	43.13	209	0.51	0.36	3.00	6.05
LHP	14.8	0.107 (0.084)[a]	42.28	204	0.50	0.34	2.53	5.91
L200	14.8	0.098 (0.077)[a]	36.79	173	0.53	0.38	3.00	4.99
L300	14.8	0.107 (0.084)[a]	42.03	203	0.50	0.34	3.18	5.85

[a] Thickness after calendering.

60.06 to 55.88 Ω corresponding to the electrodes with carbon black LHP, C45, L300, C65 and L200, respectively as shown in Fig. 6(c). Despite the electrode with C45 has relatively high electrical conductivity, it has a higher charge transfer resistance. On the contrary, although the electrode with L300 has a relatively low electrical conductivity, it has a lower charge transfer resistance. Only the electrode with L200 has the highest electrical conductivity and the lowest charge transfer resistance among these electrodes from different carbon blacks.

The ionic conductivities of the cells with different carbon blacks (κ_i) were derived from Equation (7) and are shown in Fig. 6(d).

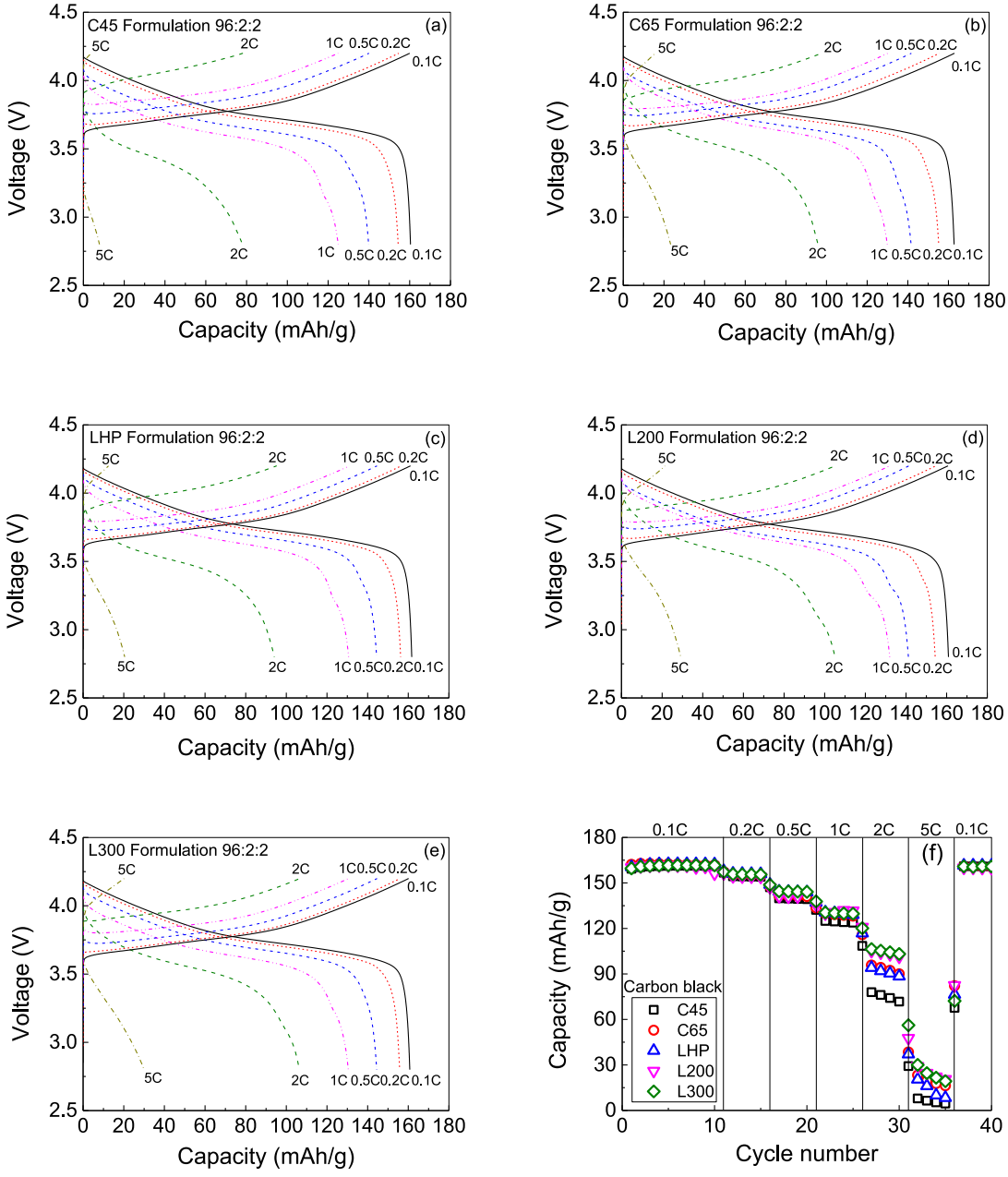

Fig. 7. Charge-discharge curves (a-e) and rate capability (f) of the electrodes based on different carbon blacks.

$$\kappa_i = \frac{1}{R_s}\frac{L_e}{A_e} \tag{7}$$

where R_s is the diameter of the cathode, L_e is the thickness of the electrode film; A_e is the area of the electrode.

The ionic conductivity is a function of porosity and tortuosity as shown in Equation (7). According to Fig. 5(c) and (d), the ionic conductivities for the electrodes with different carbon blacks should be similar. However, as can be seen from Fig. 6(d), there are some differences among them which might be attributed to electrolyte wettability [62]. Liu et al. [63] mentioned that poor electrolyte wettability leads to low ionic conductivity. Fig. 6(d) shows that there is a trend where small particle sizes of carbon black favour ionic conductivity. For example, from carbon black C45, with a particle size of 30 nm, to L300, with a particle size of 10 nm, the ionic conductivities are 0.08 and 0.15 S/m respectively. If this result takes into account the influence of carbon black particle size on the conductivity of the slurry, it is sensible to conclude that the reduction of the particle size of carbon black can increase the conductivity of the liquid (the conductivity of the slurry and the ion conductivity of the cell). The enlargement of surface area may adsorb more Li-ion and enhance the Li-ion diffusion. It might be related to electrolyte wettability and needs further investigation in the future.

It is known that the electrical conductivity of these electrodes (2–4 S/m) is approximately 10 times the ionic conductivity (0.08–0.15 S/m). Based on Drummond et al.'s simulation results [64], it is challenging to improve the battery performance by increasing electrical conductivity further because of the limitation of ionic conductivity. If further improvements in battery performance are required, the ionic conductivity must be increased correspondingly. Ionic conductivity is determined by the diffusion rate of Li-ions in the liquid electrolyte. Therefore, the constitution of the pore structure of the electrode in the next-generation NMC LIBs is more important than electrical condutivity when the electrical conductivity is 10 times higher than ionic conductivity, especially the small pore structures in the CBD which are significantly affected by carbon blacks.

3.6. Characterisation of coin half-cell performance

The discharge-charge curves for the coin half-cells with different carbon blacks are shown in Fig. 7. The curves can be divided into three parts: initial arch, plateau region and end arch corresponding to the intermediate, lithiated/delithiated, Li-rich or Li-poor phases due to the particles' bipolarization mechanism [65]. The capacity decreases as the cell is discharged and charged with increasing C-rates. All the discharge-charge curves are similar when the C-rate is less than 1 but beyond that, there is a significant change. The maximum capacity for discharging at 2C and 5C is shown in Table 2. Under the same formulation and cycling conditions, the difference in discharge capacity between the maximum value and minimum value is 1.36 times and 3.80 times at 2C and 5C caused by different carbon blacks. As such, the selection of different carbon blacks as the conductive agent causes quite different rate capabilities of the LIBs. From this result, it can be seen that carbon blacks L200 and L300 are the best choices as conductive additives for lithium-ion batteries.

The rate capability is an important factor for evaluating the performance of LIBs. Generally, efforts to improve the rate capability are carried out through carbon coating and decreasing the particle size of active materials to modify electronic and ionic conductivity [66]. The rate capability of the electrode is highly influenced by the electron transfer rate, Li-ion diffusion in the liquid electrolyte and Li-ion diffusion in the solid active material particles. Carbon black can improve the electrical conductivity and thus increase the electron transfer rate between active material particles and between the current collector and the coating film. CBD structures built by carbon black impact the Li-ion diffusion in the liquid electrolyte as well, which is related to the porosity and tortuosity of CBD. For example, although the electrode from carbon black C45 has high electrical conductivity, the CBD structure is highly porous, similar to a "sponge-like" structure, which impedes Li-ion diffusion in the electrolyte. Some researchers demonstrated that coating of TiO_2, Al_2O_3, ZrO_2 on the high-nickel NMC could improve the performance of LIBs [67]. The Li-ion diffusion is much slower in solid electroactive materials as compared to the electrolyte solution [68,69]. On the other hand, the improvement of rate capability through increasing electron transfer rate and Li-ion diffusion in the liquid electrolyte is limited by the Li-ion diffusion in the solid active particles. If the rate capability is to be further enhanced, the active material particle size should be reduced to minimise Li-ion diffusion length in the solid state [27,70].

The rate capabilities of coin half cells with different carbon blacks are shown in Fig. 7(f). At high C-rates such as 2C and 5C, the electrodes with carbon black L200 and L300 have the highest capacities, about 105 mAh/g for 2C and 30 mAh/g for 5C with corresponding capacity retentions of 60% and 14%, respectively.

To further understand the effect of carbon black and various factors determined by carbon black on battery performance, the relationships of different parameters to the capacity at a high C-rate of 5C were drawn through a statistical matrix chart as shown in Fig. 8. The purpose is to filter out the influencing parameters which have a negative or positive correlation with the discharge capacity from a large number of possible factors through blind search and find out the dominant factors. Through these findings, there is potential to identify the methods to improve the rate performance of LIBs. The justifications for selecting a high C-rate of 5C for evaluation are (i) the obvious difference in charge-discharge cycling capacity that occurs at high C-rates such as 2C and 5C; (ii) high-performance batteries need to be charged and discharged at high C-rates (above 1C), which may increase the risk of battery degradation and reduce battery lifespan, so high C-rate performance could be used to evaluate a battery. The objective of Fig. 8 is to find out the main parameters affecting battery performance and the corresponding relationship as well as the relationship with carbon black through statistics. It shows four obvious trends that lead to an increase in capacity: (i) a decrease in particle size; (ii) a decrease in I_D/I_G (i.e. more ordered graphitic carbon); (iii) an increase in storage modulus based on linear regression; (iv) a decrease in charge transfer resistance. Beyond the above four parameters, others exhibit a random relationship without a negative or positive correlation. The rate capability is not tightly related to the electrical conductivity of the electrode but is strongly relevant to the charge transfer resistance of the cell. Thus, this demonstrates that the electrochemical reaction of the NMC622 batteries is a charge transfer controlled process. The reason might be that the particle size of NMC attains approximately 1/8 of electrode thickness and the Li-ion diffusion in the solid active material particles ($\sim 10^{-15}$ m^2/s) is much lower than that in the liquid electrolyte ($\sim 10^{-8}$ – 10^{-10} m^2/s) [71]. Therefore, the electrochemical reaction in the NMC electrode is controlled by the Li-ion diffusion in the solid NMC particles, and the larger concentration difference of Li-ion between liquid electrolyte and the surface of NMC particles causes higher charge transfer resistance due to a longer solid diffusion length and much slower solid diffusion rate. In summary, among all the characteristics of carbon black, particle size and ordered graphitic carbon content are considered the most important parameters affecting the performance of lithium-ion batteries.

Table 2
Maximum discharge capacity at 2C and 5C for the electrodes with different carbon blacks.

Electrodes with different carbon blacks	C45	C65	LHP	L200	L300
Maximum discharge capacity at 2C (mAh/g)	78.0	95.8	94.1	105.1	106.4
Maximum discharge capacity at 5C (mAh/g)	7.9	23.3	20.5	29.2	30.0

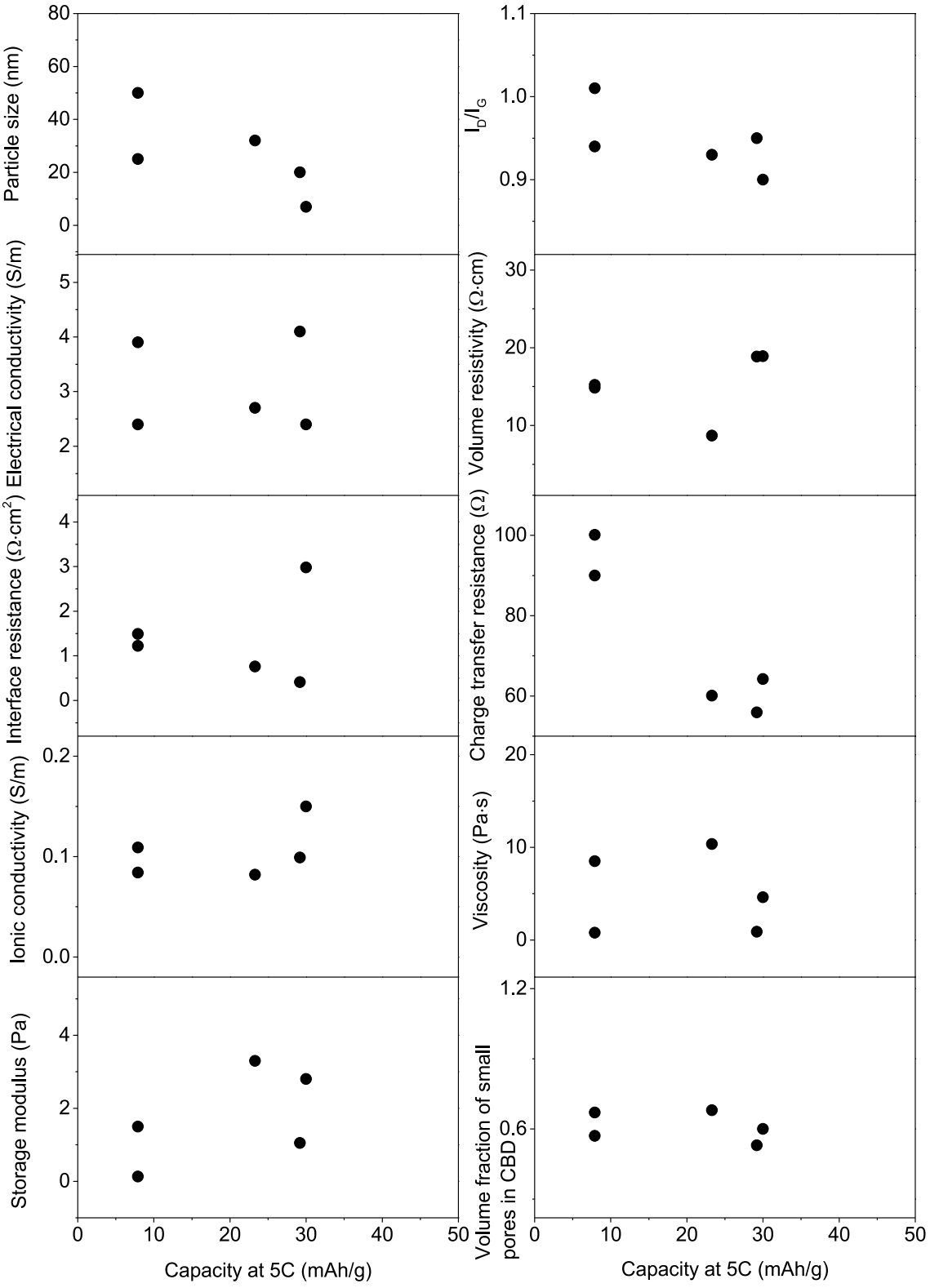

Fig. 8. Relationship of different parameters (primary particle size, I_D/I_G, electrical conductivity; interface resistance; volume resistivity; ionic conductivity; slurry viscosity; slurry storage modulus and volume fraction of small pores in CBD) to the discharge capacity of the electrodes with different carbon blacks at 5 C-rate.

4. Conclusions

Carbon black is one of the main components of the conductive binder domain in lithium-ion batteries. The selection of different carbon blacks as the conductive agent can result in a discharge capacity with a difference of 1.3–3.8 times. The normal metric used to characterise carbon black, namely, oil absorption number is not a useful predictor for lithium-ion battery applications. We have shown that the ratio of disordered carbon to ordered graphitic carbon is more useful for predicting slurry characteristics and the battery performance is directly related to the BET surface area and the ratio of disordered carbon to ordered graphitic carbon. Our conclusions and recommendations are as follows:

(i) The ratio of disordered carbon to ordered graphitic carbon mainly influences the electrical conductivity of a cast film. A higher degree of ordered graphitic carbon favours the conduction with short-range electronic contact by dry mixing and a lower degree of disordered carbon with the Raman intensity ratio of I_D/I_G less than 1 favours the conduction with the long-range electronic contact by wet mixing. The carbon black with the more disordered carbon as I_D/I_G less than 1 has a lower viscosity and storage modulus.

(ii) The BET surface area or particle size of carbon black mainly affects the pore structures, slurry conductivity and cell ionic conductivity. With the increase of BET surface area, the pore size of the small pores in the CBD becomes smaller and the pore size of the large pores in the electrodes becomes larger. As the particle size becomes smaller, the slurry conductivity and cell ionic conductivity tend to become higher. In the experimental range, the optimum BET surface area is 130–200 m^2/g corresponding to a primary particle size of 10–20 nm.

(iii) The rate capability of the NMC622 LIBs is strongly coupled with the charge transfer resistance at the surface of the NMC622 particles. Thus, the electrochemical reaction of NMC batteries is a charge transfer-controlled process.

(iv) In this study, carbon black L200 is the optimum conductive additive for NMC622 LIBs due to its corresponding electrode having the highest electrical conductivity, lowest charge transfer resistance and very high capacity at high C-rate. This conclusion only applies to NMC systems. Due to the particle size, electrical conductivity of active material particles, electrochemical reaction, the requirements of conductive additive and binder and processing method, carbon blacks need to be screened again but this work provided a research framework and methodology.

(v) Carbon-based conductive materials are an important component of LIB electrodes, which accounts for about 1–2 % of the cost of LIB, and thus it has low-cost sensitivity. With the large-scale development and industrial production of new conductive carbon materials, comprising carbon fibres, carbon nanotubes and graphene, these new conductive carbon materials could be adopted by the battery industry due to falling prices and could be widely used in the future. Currently, carbon black still remains the main conductive agent due to its compatibility with the solvent and binder, the mature carbon black industry and low price.

Carbon black is an important material that constitutes the auxiliary CBD structure for LIBs. It dictates the electron and ion transfer along with the internal resistance of the battery, so the screening of carbon black should also be considered a crucial part of the LIB manufacturing process. Based on previous scattered research work, this paper presented an in-depth systematic study of the influence of various carbon black parameters on LIBs. The research results can contribute to the screening of carbon blacks for LIB manufacturing.

CRediT authorship contribution statement

Xuesong Lu: Investigation, Methodology, Writing – original draft. **Guo J. Lian:** Formal analysis, Investigation, Writing – review & editing. **James Parker:** Formal analysis, Writing – review & editing. **Ruihuan Ge:** Formal analysis, Writing – review & editing. **Milan K. Sadan:** Formal analysis, Writing – review & editing. **Rachel M. Smith:** Supervision, Writing – review & editing. **Denis Cumming:** Conceptualization, Funding acquisition, Methodology, Project administration, Supervision, Writing – review & editing.

Declaration of competing interest

The authors declare that they have no known competing financial interests or personal relationships that could have appeared to influence the work reported in this paper.

Data availability

Data will be made available on request.

Acknowledgement

The authors thank the financial support provided by the project of Nextrode funded by The Faraday Institution, UK (Grant number: FIRG015).

Appendix A. Supplementary data

Supplementary data to this article can be found online at https://doi.org/10.1016/j.jpowsour.2023.233916.

References

[1] S. Oswald, H.A. Gasteiger, J. Electrochem. Soc. 170 (2023), 030506.
[2] J.J. Kuo, S.D. Kang, W.C. Chueh, Adv. Energy Mater. 12 (2022), 2201114.
[3] T. Knorr, S. Hein, B. Prifling, M. Neumann, T. Danner, V. Schmidt, A. Latz, Energies 15 (2022) 7821.
[4] X. Chen, W.L. Lu, C. Chen, M. Xue, Int. J. Electrochem. Sci. 13 (2018) 296–304.
[5] J. Shin, J.H. Lee, J.K. Seo, W.T.A. Ran, S.M. Hwang, Y.J. Kim, Int. J. Energy Res. 46 (2022) 16061–16074.
[6] F. Orozco, A. Salvatore, A. Sakulmankongsuk, D.R. Gomes, Y. Pei, E. Araya-Hermosila, A. Pucci, I. Moreno-Villoslada, F. Picchioni, R.K. Bose, Polymer 260 (2022), 125365.
[7] C.M. Long, M.A. Nascarella, P.A. Valberg, Environ. Pollut. 181 (2013) 271–286.
[8] F. Ma, Y. Fu, V. Battaglia, R. Prasher, J. Power Sources 438 (2019), 226994.
[9] X. Qi, B. Blizanac, A. DuPasquier, M. Oljaca, J. Li, M. Winter, Carbon 64 (2013) 334–340.
[10] S. Khodabakhshi, P.F. Fulvio, E. Andreoli, Carbon 162 (2020) 604–649.
[11] A.C. Ferrari, J. Robertson, Phys. Rev. B 61 (2000) 14095–14107.
[12] A.C. Ferrari, J. Robertson, Phys. Rev. B 64 (2001), 075414.
[13] F.C. Tai, S.C. Lee, C.H. Wei, S.L. Tyan, Mater. Trans. 47 (2006) 1847–1852.
[14] N.R. Ostyn, J.A. Steele, M. De Prins, S.P. Sree, C.V. Chandran, W. Wangermez, G. Vanbutsele, J.W. Seo, M.B.J. Roeffaers, E. Breynaert, J.A. Martens, Nanoscale Adv. 1 (2019) 2873–2880.
[15] S.-G. Kim, O.-K. Park, J.H. Lee, B.-C. Ku, Carbon letters 14 (2013) 247–250.
[16] Y.V. Surovikin, A.G. Shaitanov, V.A. Drozdov, I.V. Rezanov, A.D. Morozov, Solid Fuel Chem. 48 (2014) 392–403.
[17] H. Shi, G. Shao, B. Wu, Z. Yang, H. Zhang, P. Lv, Q. Zhu, J. Mater. Chem. A 9 (2021) 26236–26247.
[18] J.-C. Huang, Adv. Polym. Technol. 21 (2002) 299–313.
[19] X. Lu, G.J. Lian, R. Ge, J. Parker, M.K. Sadan, R. Smith, D. Cumming, Energy Technol. (2023), 2300446.
[20] B.L. Trembacki, D.R. Noble, V.E. Brunini, M.E. Ferraro, S.A. Roberts, J. Electrochem. Soc. 164 (2017) E3613–E3626.
[21] G. Liu, H. Zheng, X. Song, V.S. Battaglia, J. Electrochem. Soc. 159 (2012) A214–A221.
[22] H. Chen, M. Ling, L. Hencz, H.Y. Ling, G. Li, Z. Lin, G. Liu, S. Zhang, Chem. Rev. 118 (2018) 8936–8982.
[23] A. Narayanan, F. Mugele, M.H. Duits, Langmuir 33 (2017) 1629–1638.
[24] J.J. Richards, J.B. Hipp, J.K. Riley, N.J. Wagner, P.D. Butler, Langmuir 33 (2017) 12260–12266.
[25] L.H. Hanus, R.U. Hartzler, N.J. Wagner, Langmuir 17 (2001) 3136–3147.
[26] B. Zhao, D. Yin, Y. Gao, J. Ren, Ceram. Int. 48 (2022) 19073–19080.
[27] M.E. Spahr, D. Goers, A. Leone, S. Stallone, E. Grivei, J. Power Sources 196 (2011) 3404–3413.

[28] J.K. Mayer, H. Bockholt, A. Kwade, J. Power Sources 529 (2022), 231259.
[29] W. Bauer, D. Nötzel, V. Wenzel, H. Nirschl, J. Power Sources 288 (2015) 359–367.
[30] M. Al-Shroofy, Q. Zhang, J. Xu, T. Chen, A.P. Kaur, Y.-T. Cheng, J. Power Sources 352 (2017) 187–193.
[31] M. Wang, A.V. Le, Y. Shi, D.J. Noelle, H. Yoon, M. Zhang, Y.S. Meng, Y. Qiao, J. Mater. Sci. Technol. 32 (2016) 1117–1121.
[32] B. Marinho, M. Ghislandi, E. Tkalya, C.E. Koning, G. de With, Powder Technol. 221 (2012) 351–358.
[33] N.H. Kwon, Solid State Sci. 21 (2013) 59–65.
[34] I. Cho, J. Choi, K. Kim, M.-H. Ryou, Y.M. Lee, RSC Adv. 5 (2015) 95073–95078.
[35] J. Hwang, K. Do, H. Ahn, Chem. Eng. J. 406 (2021), 126813.
[36] X.-Y. Liu, H.-J. Peng, Q. Zhang, J.-Q. Huang, X.-F. Liu, L. Wang, X. He, W. Zhu, F. Wei, ACS Sustain. Chem. Eng. 2 (2013) 200–206.
[37] C. Gong, Z. Xue, S. Wen, Y. Ye, X. Xie, J. Power Sources 318 (2016) 93–112.
[38] K. Wang, Y. Wu, S. Luo, X. He, J. Wang, K. Jiang, S. Fan, J. Power Sources 233 (2013) 209–215.
[39] D. Pantea, H. Darmstadt, S. Kaliaguine, C. Roy, Appl. Surf. Sci. 217 (2003) 181–193.
[40] J. Entwistle, R. Ge, K. Pardikar, R. Smith, D. Cumming, Renew. Sustain. Energy Rev. 166 (2022), 112624.
[41] F.M. Smits, The Bell System Technical Journal 37 (1958) 711–718.
[42] M. Ali, L. Lin, D. Cartridge, Prog. Org. Coating 129 (2019) 199–208.
[43] X. Lu, Y. Lee, S. Yang, Y. Hao, J.R.G. Evans, C.G. Parini, J. Eur. Ceram. Soc. 30 (2010) 1–10.
[44] C.D. Reynolds, S.D. Hare, P.R. Slater, M.J.H. Simmons, E. Kendrick, Energy Technol. 10 (2022), 2200545.
[45] F. Zhang, K. Wu, X. Xu, W. Wu, X. Hu, K. Yu, C. Liang, Energy Technol. 9 (2021), 2100628.
[46] M. Takeno, T. Fukutsuka, K. Miyazaki, T. Abe, Chem. Lett. 46 (2017) 892–894.
[47] M. Mourshed, S.M. Rezaei Niya, B. Shabani, ACS Appl. Energy Mater. 5 (2022) 11413–11430.
[48] M. Mourshed, H.Q. Nguyen, B. Shabani, Materials Science for Energy Technologies 6 (2023) 290–300.
[49] J.-Z. Liang, Q.-Q. Yang, Adv. Polym. Technol. 37 (2018) 2238–2245.
[50] X. Jing, W. Zhao, L. Lan, J. Mater. Sci. Lett. 19 (2000) 377–379.
[51] G. Kraus, J.F. Svetlik, J. Electrochem. Soc. 103 (1956) 337–342.
[52] M. Chen, Q. Sun, Y. Zhou, Z. Cui, Z. Wang, W. Xing, Appl. Water Sci. 12 (2022) 161.
[53] M. Li, I. Katsouras, C. Piliego, G. Glasser, I. Lieberwirth, P.W.M. Blom, D.M. de Leeuw, J. Mater. Chem. C 1 (2013) 7695–7702.
[54] H. Bockholt, W. Haselrieder, A. Kwade, Powder Technol. 297 (2016) 266–274.
[55] J.K. Mayer, L. Almar, E. Asylbekov, W. Haselrieder, A. Kwade, A. Weber, H. Nirschl, Energy Technol. 8 (2019), 1900161.
[56] C. Meyer, H. Bockholt, W. Haselrieder, A. Kwade, J. Mater. Process. Technol. 249 (2017) 172–178.
[57] D.P. Finegan, E. Tudisco, M. Scheel, J.B. Robinson, O.W. Taiwo, D.S. Eastwood, P. D. Lee, M.D. Michiel, B. Bay, S.A. Hall, G.H. Hinds, D.J.L. Brett, P.R. Shearing, Adv. Sci. 3 (2016), 1500332.
[58] R. Ge, A.M. Boyce, Y. Shui Zhang, P.R. Shearing, D.J. Cumming, R.M. Smith, Chem. Eng. J. 465 (2023), 142749.
[59] R. Scipioni, P.S. Jørgensen, C. Graves, J. Hjelm, S.H. Jensen, J. Electrochem. Soc. 164 (2017) A2017–A2030.
[60] H. Nara, D. Mukoyama, R. Shimizu, T. Momma, T. Osaka, J. Power Sources 409 (2019) 139–147.
[61] G. Saldaña, J.I. San Martín, I. Zamora, F.J. Asensio, O. Oñederra, Energies 12 (2019) 2750.
[62] L. Zhao, Y. Li, M. Yu, Y. Peng, F. Ran, Adv. Sci. (2023), e2300283.
[63] T. Liu, X. Hu, Y. Zhang, T. He, J. Zhou, J. Qiao, Batteries 9 (2023) 166.
[64] R. Drummond, C. Cheng, P.S. Grant, S.R. Duncan, J. Electrochem. Soc. 169 (2022), 010528.
[65] A. Haghipour, M. Tahertalari, M.M. Kalantarian, Sustain. Energy Fuels 6 (2022) 879–893.
[66] M.M. Kalantarian, S. Asgari, P. Mustarelli, J. Mater. Chem. A 2 (2014) 107–115.
[67] M.J. Herzog, N. Gauquelin, D. Esken, J. Verbeeck, J. Janek, ACS Appl. Energy Mater. 4 (2021) 8832–8848.
[68] A. Eftekhari, ACS Sustain. Chem. Eng. 5 (2017) 2799–2816.
[69] S.K. Mylavarapu, F. Ulu Okudur, S. Yari, D. De Sloovere, J. D'Haen, A. Shafique, M. K. Van Bael, M. Safari, A. Hardy, ACS Appl. Energy Mater. 4 (2021) 10493–10504.
[70] S.-L. Wu, W. Zhang, X. Song, A.K. Shukla, G. Liu, V. Battaglia, V. Srinivasan, J. Electrochem. Soc. 159 (2012) A438–A444.
[71] C.H. Chen, F.B. Planella, K. O'Regan, D. Gastol, W.D. Widanage, E. Kendrick, J. Electrochem. Soc. 167 (2020), 080534.